

**Figure 1.** Normalized distance  $\langle z_{b,end} \rangle / (N_b \bar{l}_b)$  of the end-monomer of an adsorbed chain ( $\varepsilon = 1.5$ , far above the adsorption transition which occurs at  $\varepsilon \approx 1.0$ ; note that energies are quoted in units of the thermal energy  $k_B T = 1$  throughout) versus force, for  $N_b = 67$ . For five states typical configuration snapshots are shown. No side chains are present here ( $N = 0$ ).

such as the number of adsorbed monomeric units, distance of the free end of the macromolecule (considering always one end being grafted) from the substrate, parallel and perpendicular linear dimensions of the polymer, etc. We vary the speed of increase (or decrease, respectively) of the force over 3 orders of magnitude, to elucidate the presence (or absence, respectively) of hysteretic behavior. For the sake of comparison, also corresponding results for simple linear chains (without side chains) are presented. Section four summarizes our conclusions.

## 2. MODEL AND SIMULATION METHODS

As in our previous work on simulations of bottle-brush polymers,<sup>37–41</sup> we use the bond fluctuation model on the simple cubic lattice<sup>50–52</sup> to describe both the “backbone polymer” and the side chains that are grafted to it. In this model, effective monomers are represented by elementary cubes which block all eight corner sites of the cube for further occupation, to model the excluded volume interaction. Empty lattice sites account for the solvent implicitly. The effective bonds connecting such effective monomers along a chain are chosen from a set of “bond vectors”, namely  $\{[2,0,0], [2,1,0], [2,1,1], [2,2,1], [3,0,0], \text{ and } [3,1,0], \text{ respectively}\}$ , including also all possible permutations and assignments of positive or negative signs to these coordinate differences (the lattice spacing being our unit of length). Remember that each effective bond can be taken to represent a group of about three to five carbon–carbon covalent chemical bonds along the chain molecule; in a crude way the variability in the length of the effective bond is thought to represent the local conformational degrees of freedom due to the various minima in the torsional potential of a chemically realistic description of a polymer. Noting that the average length of an effective bond turns out to be about  $\bar{l}_b = 2.7$  lattice spacings, one finds that for polymers such as a polyethylene, polystyrene, etc. a lattice spacing would roughly correspond to about 0.2–0.3 nm.<sup>37</sup> Apart from excluded volume, no other intermolecular interaction between effective monomers is included (although this could be done,<sup>51</sup> if desired).

We use this model for both the backbone chain and the side chains, ignoring the difference in chemical structure occurring for real bottle-brush polymers<sup>33–36</sup> between side chains and backbone. Similar to experiment, we graft one side chain to every effective monomer of the backbone, apart from the first and last one; the first monomer of the backbone is grafted to the substrate (this means, the  $z$ -coordinate of the four lower corners of the cube is  $z = 0$ , and their  $x, y$  coordinates are kept fixed as well), while the pulling force acts on the last monomer only. Unlike experiment,<sup>20</sup> where also interior parts of a bottle-brush polymer can bind to an AFM tip, the simulation setup hence does not suffer from any ambiguities about the question on which effective monomers the pulling force acts. Because of the chemical grafting, the chains can, however, not detach completely from the surface, a phenomenon which was recently studied both theoretically and by simulations.<sup>53,54</sup> In the bulk the backbone chain length  $N_b$  was varied from  $N_b = 67$  to  $N_b = 1027$ , and the side chain length  $N$  typically up to  $N = 24$  (for a few cases also  $N = 36$  and  $48$  was considered).<sup>37–39</sup> Adsorbed chains (effective monomers are adsorbed and experience an energy  $\varepsilon$  when they have the lower four corners of the cube in the plane  $z = 0$ ) are more difficult to equilibrate, and hence the largest adsorbed bottle brush that could be simulated<sup>40,41</sup> was characterized by  $N_b = 643$ ,  $N = 18$ . Note that the energy parameter enters the transition probability for Monte Carlo moves via the Boltzmann factor  $\exp[-\Delta E/k_B T]$ , where  $k_B T$  (chosen unity here) is the thermal energy and  $\Delta E$  the energy change due to the move. We apply here the standard Metropolis algorithm of Monte Carlo simulation.<sup>55</sup> As Monte Carlo moves, we use both local moves<sup>50–52</sup> (where one attempts to displace a randomly chosen monomer by one lattice unit in a randomly chosen direction; of course, moves that would lead to occupied sites below the surface plane ( $z < 0$ ) are always rejected) as well as moves where a monomer can “hop” to a more distant site (“L26 algorithm”<sup>56</sup>). This move violates the condition (that is desirable when one wishes to apply the model for a study of entangled polymer dynamics) that chains in the course of their motions cannot intersect, but speeds up the equilibration significantly. For the study of adsorbed chains in equilibrium, also pivot moves<sup>40,41,57</sup> were used. Note that the force  $f$  enters the simulation only when the

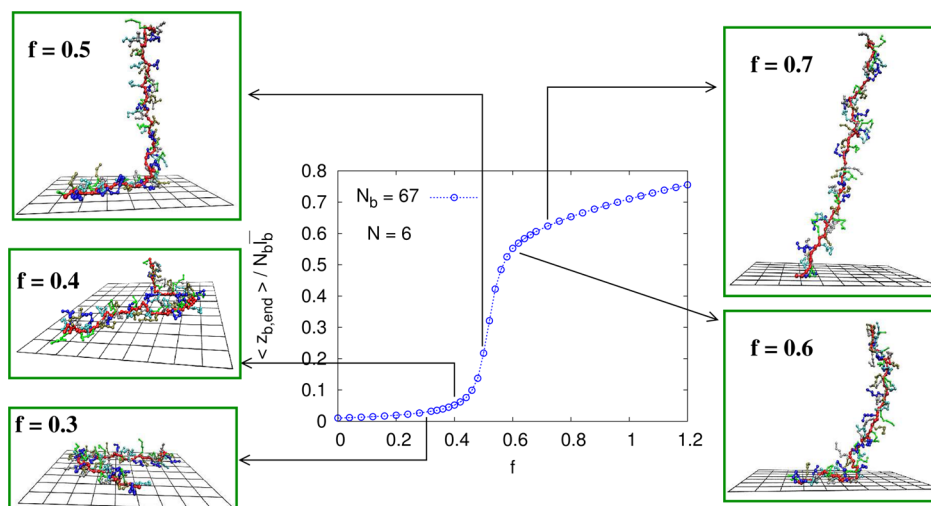


Figure 2. Same as Figure 1, but for side chains of length  $N = 6$ .

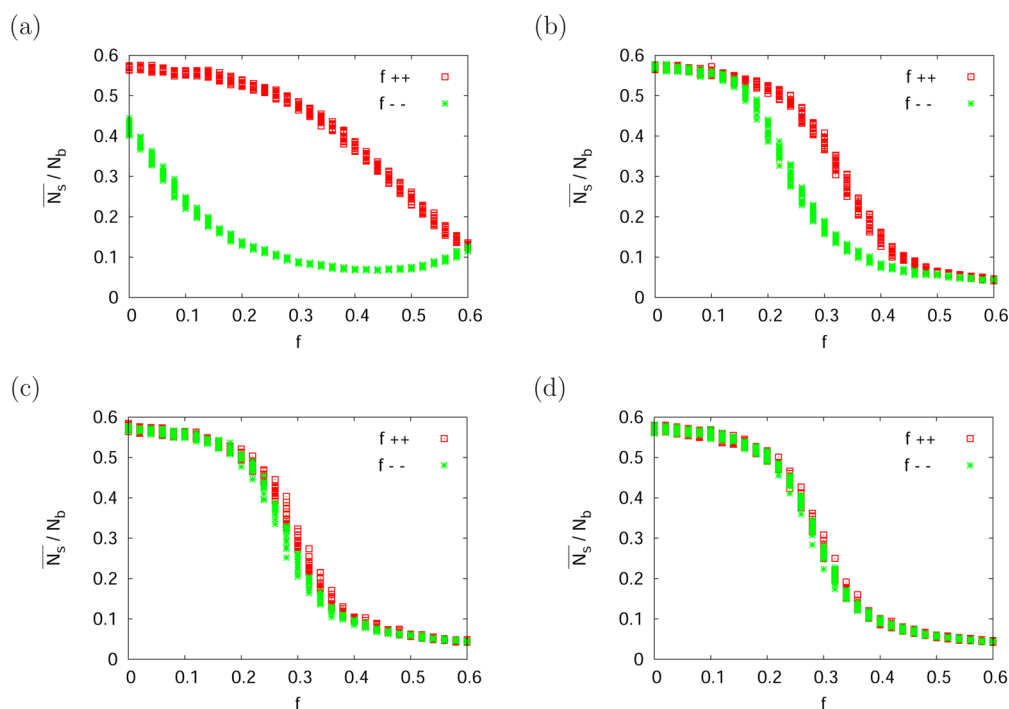
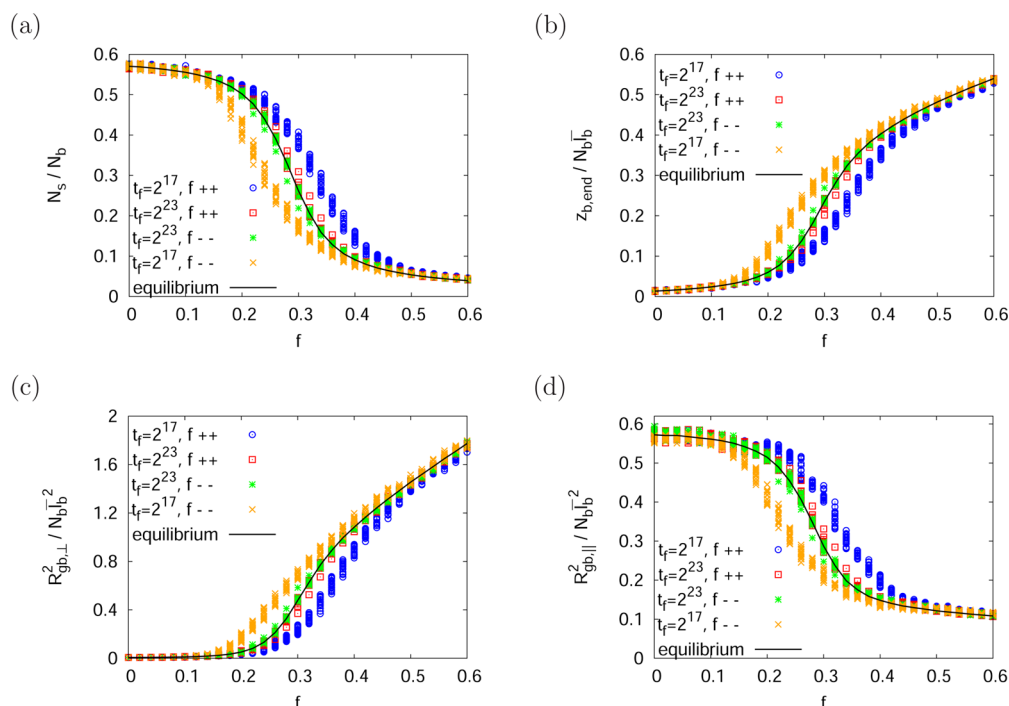


Figure 3. Fraction of adsorbed monomer-surface contacts,  $\overline{N}_s / N_b$  for linear polymer chains of length  $N_b = 67$ , plotted vs force  $f$ , using 512 independent runs when the force  $f$  is increased ( $f++$ ) or decreased ( $f--$ ) in steps  $\Delta f = 0.02$ , starting at  $f = 0$  and ending at  $f = 0.6$ . The spread in the symbols indicate the fluctuations from run to run. At each step of  $f$  the force is kept constant over a time of  $t_f$  MCS, with  $t_f = 2^{14}$  (a),  $2^{17}$  (b),  $2^{20}$  (c), and  $2^{23}$  (d).

$z$ -coordinate of the last monomer changes by  $\Delta z$ , via an additional Boltzmann factor  $\exp[-f\Delta z/k_B T]$  in the transition probability. Of course, this algorithm provides only a crudely simplified description of polymer dynamics,<sup>37,38</sup> in particular, hydrodynamic interactions provided by the solvent are completely missing, and so the description of dynamical phenomena is essentially on the level of the Rouse model.<sup>57–59</sup> However, the Rouse model<sup>59</sup> is broadly considered and is useful to provide a first orientation on polymer dynamics.<sup>57–59</sup>

As an example, Figures 1 and 2 show typical data on the equilibrium distance  $\langle z_{b,end} \rangle$  of the end-monomer of the backbone versus the force  $f$ , for a polymer with no side chains (Figure 1) and a bottle-brush with side chain length  $N = 6$  (Figure 2). While  $N = 6$  clearly means the side chain is very

short, it does correspond to the range of side chain lengths considered in experiments.<sup>35,36</sup> One recognizes a pronounced sigmoidal character of these extension versus force curves, with three regions, illustrated by the snapshots: in the region of small  $f$  (i.e.,  $f/k_B T \leq 0.25$  in Figures 1 and 2) the macromolecule essentially stays fully adsorbed, irrespective of the pulling. Then there is a region of intermediate  $f$ , where a steep rise occurs; there part of the chain is still adsorbed, another part is already pulled off. In the final part the curve gradually flattens: then basically no adsorbed part exists any longer, but the chain (in the case where no side chains are present,  $N = 0$ ) still is a bit coiled on the local scale, and much stronger forces are needed to stretch the chain to its maximum



**Figure 4.** Comparison of data obtained for  $t_f = 2^{17}$  and  $t_f = 2^{23}$  (similar as shown in Figure 3) with well-equilibrated data shown as curves, where for each value of  $f$  averages over  $2.5 \times 10^5$  independent configurations are measured every  $2^{16}$  MCS. Data shown are the fraction of adsorbed surface contacts,  $\overline{N}_s/N_b$  (a), rescaled height of the free end monomer,  $z_{b,\text{end}}/(N_b \overline{l}_b)$  (b), rescaled mean square gyration radius perpendicular (c) and parallel (d) to the surface,  $R_{\text{gb},\perp}^2/(N_b \overline{l}_b^2)$  and  $R_{\text{gb},\parallel}^2/(N_b \overline{l}_b^2)$ , respectively.

length (corresponding to  $\langle z_{b,\text{end}} \rangle / N_b \overline{l}_b = 1$ ). In the case of the bottle-brush polymers the snapshots (both of the pulled chains and of fully adsorbed chains, see<sup>40,41</sup>) are really suggestive of a description by the worm-like chain model, and the same observation has been made for the experiment.<sup>20</sup> However, one needs to be more careful: the analyses presented in<sup>38,39,60</sup> clearly showed that the popular Kratky–Porod model<sup>61</sup> for semiflexible polymers is not an accurate description for bottle-brush polymers, since their large persistence length  $l_p$  is caused by a rather large “chain thickness” (one can estimate that  $l_p \approx 3(\langle R_{\text{cs}}^2 \rangle)^{1/2}$ , where  $R_{\text{cs}}$  is the cross-sectional radius of the bottle-brush<sup>62</sup>) and it was shown in refs 38, 39, and 60 that in this case the Kratky–Porod model is not applicable.

### 3. SIMULATION RESULTS

**3.1. Pulling Single Chains without Side Chains off a Flat Surface.** In Figures 3 and 4, we characterize our pulling experiment by looking at the number of adsorbed monomers (Figure 3 and Figure 4a), the height of the end monomer above the surface (Figure 4b), and the extension of the chain perpendicular ( $R_{\text{gb},\perp}^2$ , Figure 4c) and parallel to the surface ( $R_{\text{gb},\parallel}^2$ , Figure 4d). All data are obtained for a short linear chain ( $N_b = 67$ ) under conditions where in the absence of pulling forces it is strongly adsorbed (we work at  $\varepsilon = 1.5$  throughout). We consider in each case time series where the pulling force  $f$  is either increased ( $f++$ ) or decreased ( $f--$ ) in increments of  $\Delta f = 0.02$ . To model variable pulling speed, the force is kept constant for  $t_f$  Monte Carlo steps (MCS) at each step,  $t_f/t_s = 64$  data points are stored every  $t_s$  MCS for a constant force. Average values taken from 512 independent runs are shown. Here by the overbar ( $\overline{\quad}$ ) we mean a sampling over many nonequilibrium trajectories, unlike a sampling  $\langle \dots \rangle$  over an

equilibrium distribution. We clearly see that when we pull too fast (holding the chain at each value of  $f$  only  $2^{14}$  MCS), the systems falls completely out of equilibrium, and when we turn from  $f = 0.6$  to  $f = 0$  again, we end up in a only partially adsorbed nonequilibrium conformation (Figure 3a). It then also happens that the decrease of  $f$  near  $f = 0.6$  does not lead to an increase of  $N_s/N_b$  and  $R_{\text{gb},\perp}^2$  (and a decrease of  $z_{b,\text{end}}$ ,  $R_{\text{gb},\parallel}^2$ ), but rather the system develops opposite to what one expects, so the curves for decreasing  $f$  are nonmonotonic (see Figure 3a). For somewhat larger  $t_f$  ( $t_f = 2^{17}$ ), this anomalous behavior typical for far from equilibrium simulations is gone, but we still see a pronounced hysteresis between the data for ascending and descending force. Only for the largest choice of  $t_f$  ( $t_f = 2^{23}$ ) hysteresis has disappeared completely, ascending and descending branch superimpose within error, equilibrium along the full process has been reached. This assertion is also confirmed when we compare the latter data with calculations where we take averages at extremely long runs at fixed values of  $f$  (full line in Figure 4) where it can be anticipated that well-equilibrated simulation results have been obtained, which is proven by a detailed analysis of “time correlations” in the “time series” of these runs.

In the following, we also briefly discuss the choices made for the step size of the force for our ramping protocol. For the discrete ramping protocol necessary in the Monte Carlo simulation, both the size of the step in the applied force and the duration of application of this force are relevant. The step size was selected so as to give a fine enough discretization of the complete force interval, while still allowing for sufficiently large duration of application of this force. As is shown in Figure 3a, for a too short duration severe nonequilibrium effects distort the simulation results. So the quality of the statistics obtainable at minimal duration of the steps necessary and number steps

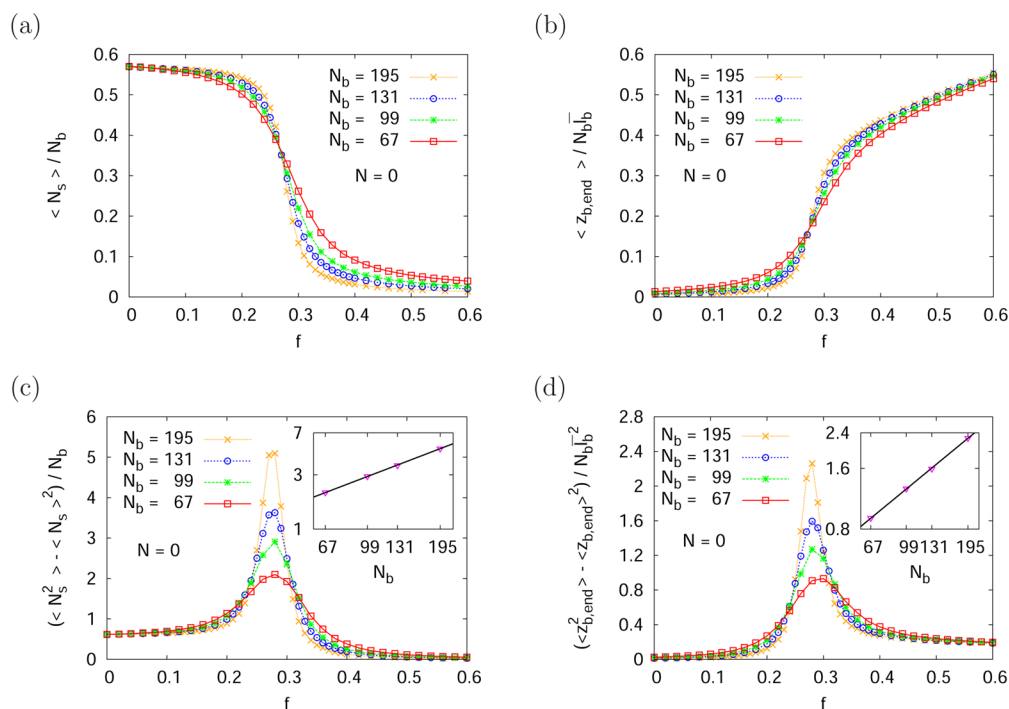


**Figure 5.** Fraction of monomer–surface contacts  $\langle N_s \rangle / N_b$  (a), average height of the end monomer  $\langle z_{b,end} \rangle / (N_b \bar{l}_b)$  (b), and the reduced variances of these quantities,  $(\langle N_s^2 \rangle - \langle N_s \rangle^2) / (N_b \bar{l}_b^2)$  (c), and  $(\langle z_{b,end}^2 \rangle - \langle z_{b,end} \rangle^2) / (N_b \bar{l}_b^2)$  (d), plotted vs the force  $f$ . Data for  $N_b = 67, 99, 131,$  and  $195$  are included, as indicated. In parts c and d, the maximum values of the reduced variances are shown in the insets, plotted vs  $N_b$  in a log–log scale. The straight lines of slope 0.83 (c) and 0.85 (d) give the best fit of the data.

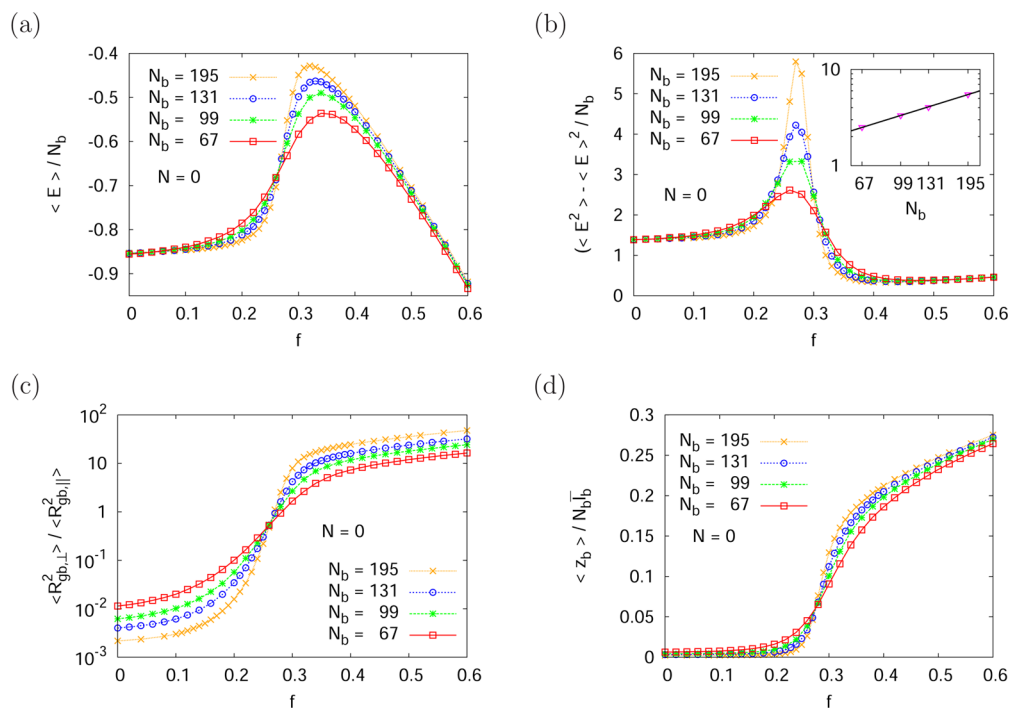


**Figure 6.** Average energy  $\langle E \rangle / N_b$  per monomer (a) and its normalized variance  $(\langle E^2 \rangle - \langle E \rangle^2) / N_b$  (b), ratio between the mean square gyration radius component perpendicular and parallel to the surface,  $\langle R_{gb,\perp}^2 \rangle / \langle R_{gb,\parallel}^2 \rangle$  (c), and average normalized distance of the monomers of the chain from the surface,  $\langle z_b \rangle / (N_b \bar{l}_b)$  (d). Data for  $N_b = 67, 99, 131,$  and  $195$  are included, as indicated. Note that the energy  $E$  included also the term  $-fz_{b,end}$  due to the force. In (b) the heights of the peaks plotted vs  $N_b$  in a log–log scale are shown in the inset. The straight line of slope 0.74 gives the best fit of the data.

possible led to the choice of (mostly)  $\Delta f = 0.02$  for the simulations. Of course, the time  $t_f$  which we have used, from  $2^{14}$  to  $2^{23}$  MCS, needs to be related to the intrinsic relaxation times

of macromolecules. Defining for a free chain in  $d = 3$  dimensions in dilute solutions a relaxation time  $\tau_1$  via<sup>63</sup> the condition that the time-dependent mean square monomer

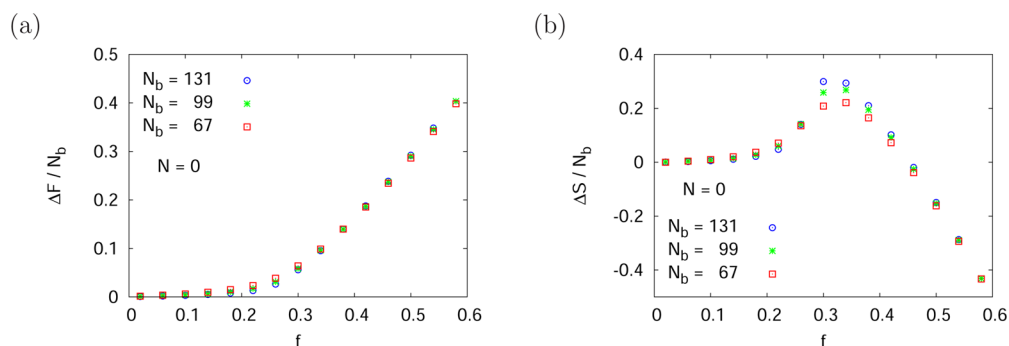


**Figure 7.** (a) Plot of the free energy per monomer  $\Delta F/N_b$  (relative to the free energy at  $f=0$ ) obtained from thermodynamic integration  $\Delta F(f)/N_b = \int_0^f df' \langle z_{b,\text{end}}(f') \rangle$ , where  $z_{b,\text{end}}(f')$  is the  $z$ -component of the position of the monomer at which the pulling force  $f'$  acts. Three chain lengths are included as indicated. (b) Entropy difference computed from Figures 6a and part a) according to  $\Delta S = \Delta E - \Delta F$  where  $\Delta E = E(f) - E(0)$ .

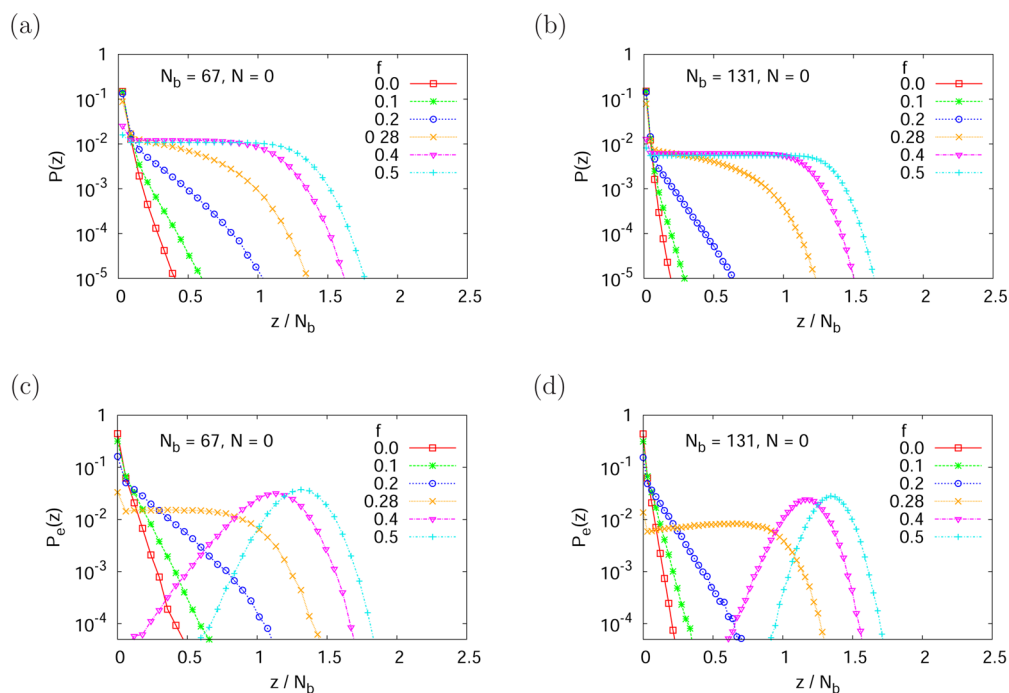


**Figure 8.** Distribution function  $P(z)$  of all monomers of the chains (a, b) and of the end monomers  $P_e(z)$  (c, d), for  $N_b = 67$  (a, c) and 131 (b, d). Six choices of  $f$  are included, as indicated.

displacement becomes equal to the mean square gyration radius, one finds  $\tau_1 \approx \tau_0 N^\nu$  with  $\tau_0 \approx 2$  and  $z = 2.24$  (the theoretical value of  $z$  would be  $z = 2\nu + 1 \approx 2.18$ , with  $\nu$  the Flory exponent<sup>57–59</sup>) while for  $N = 67$  the resulting time ( $\tau_1 \approx 25000$ ) is clearly smaller than the times  $t_f = 2^{17}, 2^{20}$ , and  $2^{23}$ , it is remarkable that Figures 3 and 4 still reveal some hysteresis: this is due to some “critical slowing down”<sup>55</sup> associated with the phase transition from the adsorbed chain to the desorbed mushroom, which appears in the limit  $N \rightarrow \infty$ . Note that this transition is believed to be weakly of first order (no free energy barrier separating the coexisting states<sup>64</sup>) and hence critical slowing down is expected. The quoted time constant  $\tau_0$  refers to the “random hopping” algorithm, where monomer moves by one lattice spacing are attempted, and due to our usage of  $L = 26$  moves and pivot moves  $\tau_1$  would be even smaller.<sup>40,41</sup> However, due to the slow desorption kinetics, we had to restrict attention to  $N_b \leq 195$  here to avoid excessive amounts of computer resources for getting well equilibrated results.

Similar data as shown in Figures 3 and 4 have also been generated for longer chains ( $N_b = 99, 131$  and  $195$ ,

respectively), but in order to save space, they are not shown here; rather we focus on the equilibrium behavior of the chain as a function of the force in Figures 5 and 6, where we compare all four chain lengths that were studied. Recall that the Monte Carlo simulations performed here can describe dynamic aspects of the pulling process only qualitatively, due to various simplifications inherent in our simulation (we pull at constant force that is stepwise increased rather than at constant velocity of a bead harmonically coupled to the end monomer, we omit hydrodynamic forces transmitted via the solvent; we ignore that the chain must not intersect itself in the course of its motions). But the static equilibrium behavior is a reasonable description of a real chain under the action of a force, since one can justify the present model in terms of a coarse-graining where several chemical bonds along the chain backbone are lumped into a single effective bond.<sup>57,58</sup> One can see that with increasing chain length  $N_b$  the transition from the adsorbed chain to the almost fully stretched state of the mushroom becomes sharper. It is tempting to interpret this force-induced desorption as a first-order transition rounded by “finite size” (i.e., finite chain

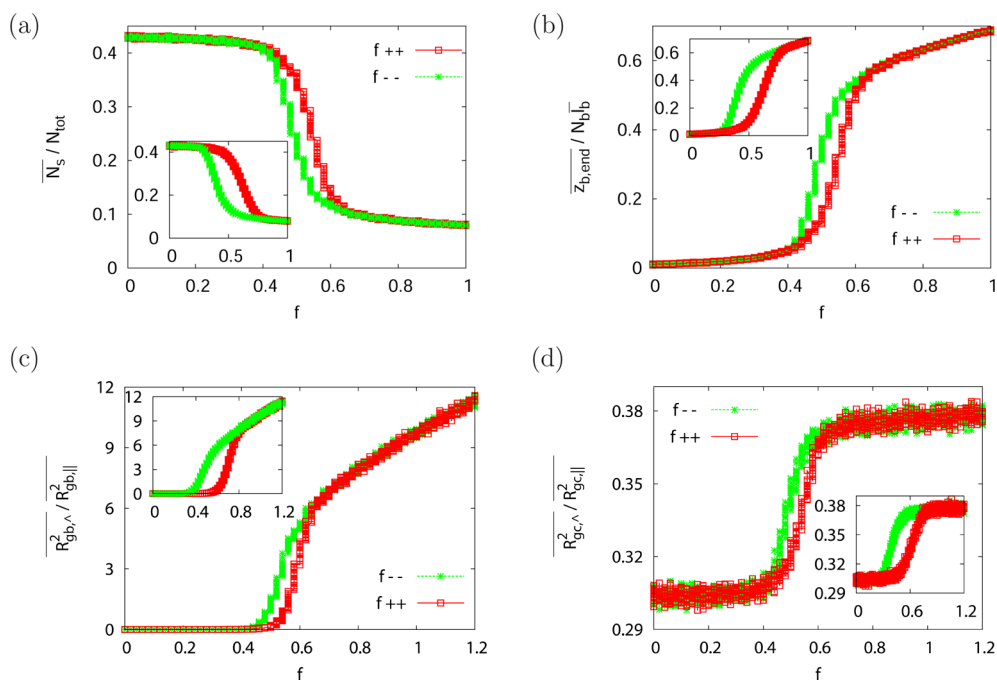


**Figure 9.** Fraction of adsorbed monomer-surface contacts,  $\overline{N}_s/N_{tot}$  (a), the normalized end monomer position,  $\overline{z}_{b,end}/(N_b \overline{l}_b)$  (b), the ratio between the mean square gyration radius component perpendicular and parallel to the surface for the backbond monomers,  $\overline{R}_{gb,\perp}^2/\overline{R}_{gb,\parallel}^2$  (c), and for the side chain monomers,  $\overline{R}_{gc,\perp}^2/\overline{R}_{gc,\parallel}^2$  (d), plotted vs the force  $f$  (incremented in steps of  $\Delta f = 0.02$ , as in Figure 3, keeping  $f$  constant over a time interval of  $t_f$  MCS, here  $t_f = 2^{23}$ ) for a bottle-brush polymer with backbone chain length  $N_b = 67$  and side chain length  $N = 6$ . In the insets the same data are shown for runs keeping the force constant over  $t_f = 2^{20}$  MCS.  $t_f/t_s = 64$  data points are stored every  $t_s$  MCS for a constant force, and average values from 512 independent runs are shown. Note that both runs with increasing ( $f++$ ) and decreasing ( $f--$ ) force were made, as indicated.

length  $N_b$ ). Similar conclusions were reached for different models in the literature.<sup>47–49</sup> According to this interpretation, the height of the peaks in Figures 5c, 5d, and 6b should increase linearly with  $N$ ; however, the log–log plots shown in the insets reveal that the asymptotic regime of this scaling has not been reached yet. In Figure 7a, we present the free energy change  $\Delta F(f)$  obtained from thermodynamic integration as a function of pulling force. From this and the result for the energy shown in Figure 6a, the entropy change  $\Delta S(f)$  associated with this transition shown in Figure 7b is obtained. We see that the entropy change also develops toward an entropy jump in the limit  $N \rightarrow \infty$ , like in the internal energy  $E$  (Figure 6a). The intersection points of the entropy curves, and the positions of the maxima in Figures 6b, 5c, 5d are compatible with each other, indicating that the transition point for  $N_b \rightarrow \infty$  will occur at about  $f = f_t \approx 0.27 \pm 0.01$ .

The character of this transition is also very distinctly shown by the behavior of the distribution function of the monomer density  $P(z)$  and the end monomer density  $P_e(z)$  for different forces, respectively (Figure 8). One sees that in the partially desorbed state (e.g.,  $f = 0.2$ ) the distributions are superpositions of two exponentials: at very small  $z$  a rapidly decaying part dominates (only this part is present for  $f = 0$ , of course); then a much slower decay follows, which reflects the strong fluctuations of the “interface” between the still adsorbed part and the already desorbed part of the chain (recall that this interface is a single monomer only: therefore, the first-order transition that emerges for  $N_b \rightarrow \infty$  does not have a free energy barrier between the coexisting states.<sup>32,64</sup> Thus, the distribution function  $P_e(z)$  of the free end switches from the slow exponential decay to the Gaussian distribution with a  $\langle z_{b,end} \rangle /$

$N_b$  of order unity without showing a double-peak distribution in between: rather one obtains a distribution which is almost flat over a significant region of  $z$ , for the value of  $f$  where the fluctuations are maximal.

**3.2. Pulling a Bottle Brush.** How is the phenomenology developed in the preceding discussion changed when we go from a linear chain to a bottle brush polymer? In Figure 9 we show the counterparts of Figure 4 for a small bottle-brush polymer of the same backbone chain length ( $N_b = 67$ ) and with side chain length  $N = 6$ . The first thing to note is an increase of the intrinsic relaxation times of these chains leading to a hysteresis behavior which is even more pronounced than for linear chains. Therefore, only the two slower choices of changing the force  $f$  are shown,  $t_f = 2^{20}$  and  $t_f = 2^{23}$ , respectively. For smaller choices of  $t_f$ , the system is very strongly out of equilibrium. Second, the force necessary to desorb the bottle brushes is larger compared to the linear chains (from the hysteresis loops one can estimate  $f_t \approx 0.5$  compared to  $f_t = 0.27$  for the linear chains).

As was already suspected from a comparison of Figures 1 and 2, the presence of the side chains of the bottle-brush polymer leads to a more abrupt character of the force-induced desorption. In this context, it is also instructive to study how the force-induced desorption changes the side chain conformations. We find that for the adsorbed chains, side chains have slightly smaller perpendicular (by 16%) and slightly larger parallel (by 8%) mean square radii than in the desorbed case. In Figure 9d) we show the ratio of the perpendicular and parallel extension of the side chains for the same two pulling speeds considered in the previous figures and this ratio marks the desorption transition as clearly as the corresponding ratio for

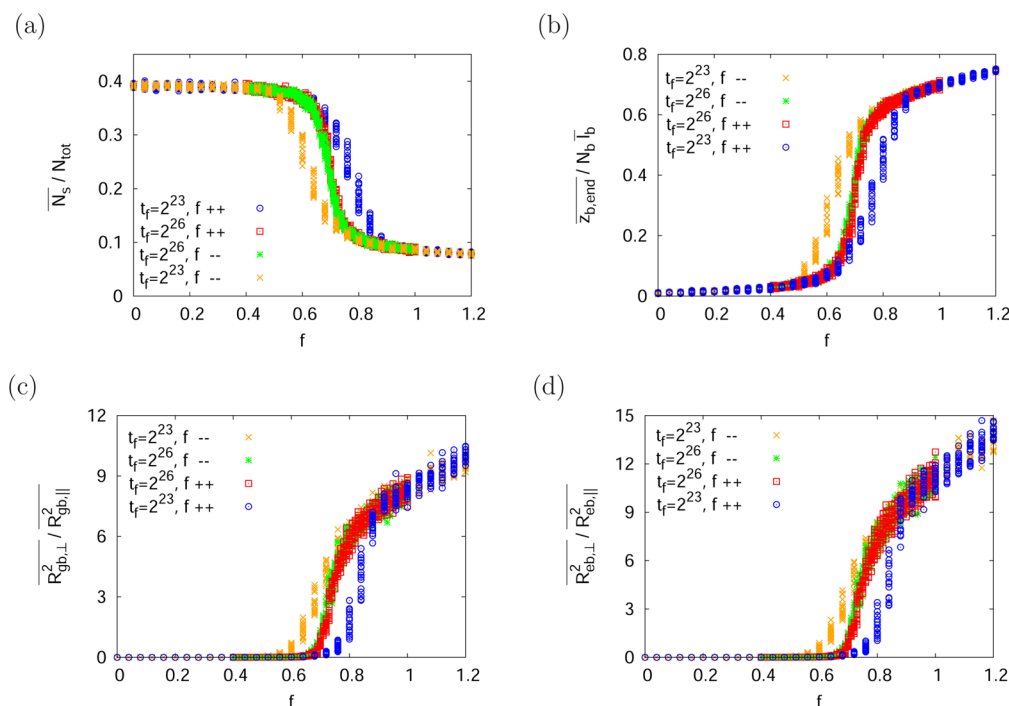


**Figure 10.** Fraction of monomer-surface contacts  $\overline{N_s}/N_{tot}$  (a), height of the end monomer  $\overline{z_{b,end}}/N_b \overline{l_b}$  (b), ratio between the mean square gyration radius components perpendicular and parallel to the surface (c), and ratio between the mean square end-to-end distance components perpendicular and parallel to the surface (d). Average values from 128 independent runs are shown for  $N_b = 67$ ,  $N = 12$ . Two sets of parameters are chosen here, ( $t_f = 2^{23}$ ,  $\Delta f = 0.04$ ,  $0 \leq f \leq 1.2$ ), and ( $t_f = 2^{26}$ ,  $\Delta f = 0.01$ ,  $0.4 \leq f \leq 1.0$ ).

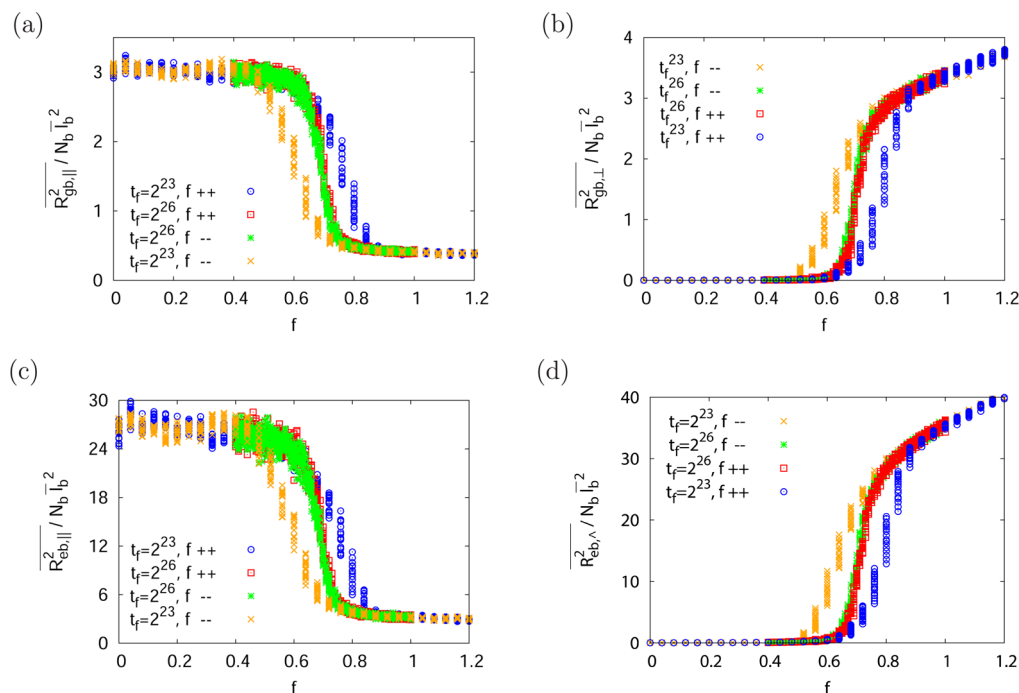


**Figure 11.** Mean square gyration radius in the direction parallel to the surface,  $\overline{R_{gb,\parallel}^2}/N_b \overline{l_b}^2$  (a), and perpendicular to the surface,  $\overline{R_{gp,\perp}^2}/N_b \overline{l_b}^2$  (b) for the same parameters as in Figure 10. (c, d) Same as parts a) and b), but for the mean square end-to-end distance.

the backbone. This entails that the edge between adsorbed and desorbed part of the chain is no longer just given by a single monomer, but adsorbed side chain monomers contribute to this as well. Still, for finite side chain length, there is no extensive number of monomers to be pulled off the surface at the transition, so that the weakly first order nature of the

transition is not supposed to change, although it will sharpen and shift with increasing side chain length. In Figures 10 and 11, we show that these expectations are borne out. The variation at the transition does indeed become sharper when the length of the side chains is increased from  $N = 6$  to  $N = 12$  and the transition for  $N = 12$  is around  $f_t \simeq 0.7$ . Since at the

same time, however, relaxation times become larger, smaller pulling speeds ( $t_f = 2^{23}$  and  $2^{26}$ ) needed to be used. The latter is almost sufficient to exhibit reversible desorption and readorption behavior for the combination of backbone ( $N_b = 67$ ) and side chain ( $N = 12$ ) length employed in Figures 10 and 11.

Let us finally compare our results to the experimental observations as reported for bottle brush polymers in ref 20. The experimental curves of force versus extension as presented in Figures 3 and 4 of this work correspond to the data we present in Figures 9b and 10b rotated by 90 deg. The first obvious difference to the experimental data is that the steep increase in extension occurs at a finite pulling force in the simulation, whereas in the experimental figures, the extension occurs at force zero. We believe this to be an artifact of the force calibration in the experiment. The experiment is done on strongly adsorbed bottle brush polymers, so there has to be a first-order desorption transition at a finite pulling force, not at force zero. With the calibration done in the experiment, all information on the desorption transition of the polymers is removed from the data. The next thing to observe is that the increase of extension at the desorption transition is much steeper than in the simulation, which can be attributed to the larger chain lengths studied experimentally. As discussed above, our data indicate a steepening of the slope in this region with increasing backbone as well as side chain length. Lastly, the extension of the bottle-brush polymers after desorption is analyzed in the experiments using an equation derived for a polymer model with extensible backbone<sup>65</sup>

$$\frac{\bar{z}_{b,\text{end}}}{N_b \bar{l}_b} = 1 - \frac{1}{2} (f_p)^{-1/2} + \frac{f}{\Phi} \quad (1)$$

where  $\Phi$  is the elastic stretch module of the chains and where we have equated the contour length,  $L = N_b \bar{l}_b$ . We perform this type of analysis in Figure 12 which compares the force

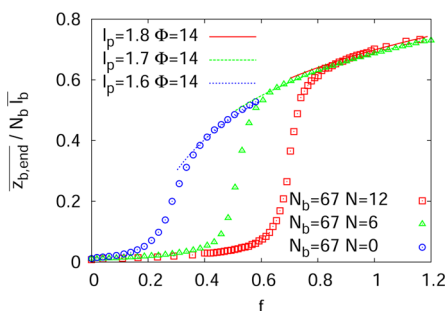


**Figure 12.** Extension–force curves for a linear chain ( $N = 0$ , blue circles) and two bottle brush polymers with backbone length  $N_b = 67$ : ( $N = 6$ , green triangles, and  $N = 12$ , red squares). The curves in all cases are fits to an extensible chain model (see text).

extension curves of the linear chains with  $N_b = 67$  to the bottle brushes with  $N_b = 67$  and  $N = 6$  and  $N = 12$ . The fits in all cases are only able to describe the final part of the data at large force. Interestingly, this part of the extension curve for the bottle brush is almost the continuation of the corresponding part for the linear chain (i.e., if we would have continued pulling the linear chain to larger force these curves would basically overlap). The fit parameters for the persistence lengths are very similar (1.6, 1.7, and 1.8, with an error of about 0.05 in all cases) and they correspond to values for a flexible backbone ( $l_p/l_b < 1$ ), the bottle-brushes showing slightly larger stiffness in

this pulling regime. Note that the values of the persistence length  $l_p$  in such a fit have, however, nothing to do with the persistence length describing the (local) stiffness of the unstretched bottle brush, which is an order of magnitude larger.<sup>37–39</sup> The values for the elastic stretch modulus agree. The picture which emerges from these findings is that the presence of adsorbed side chain monomers shifts the desorption transition to higher force, but once a backbone part and its attached side chains are desorbed, it is only the backbone which is mechanically active and resists the stretching force (at least for the short side chain lengths we could study).

#### 4. CONCLUSIONS

In this paper, the process where an adsorbed polymer chain or an adsorbed bottle brush polymer is pulled off from a surface by applying a force until the macromolecule takes a mushroom configuration, is simulated by Monte Carlo methods. We consider also the reverse process, where the force acting on the stretched mushroom is gradually decreased again and larger and larger parts of the macromolecule get reabsorbed. We pay particular attention to the effects of varying the speed with which the strength of the force is increased (or decreased, respectively). It is shown that this speed has to be extremely small to prevent that the system falls out of equilibrium and hence ensure that the changes of state of the macromolecule are reversible. If the speed is a bit too fast in order that the system stays in equilibrium throughout, we observe a hysteresis loop in all variables of interest (fraction of adsorbed monomers, distance of the chain end from the surface, parallel and perpendicular mean square gyration radii components). If the pulling speed is much too fast, the system is falling completely out of equilibrium, and when one then decreases the force again one finds the counterintuitive result that the distance of the end from the surface may further increase a while, although the force decreases. In such a case, the final state (where again no force is applied, as in the starting state) is an only incompletely adsorbed polymer (Figure 3a).

We find that the extension versus force curve in general is S-shaped and the maximum slope in the center of this variation increases with chain length (and it also increases with increasing length of side chains when one considers instead of a linear chain a bottle brush polymer with the same backbone chain length as the linear chain). Theoretically, it has been established<sup>32,47–49,64</sup> that in the limit of infinite chain length the desorption transition becomes a sharp phase transition (of first order). Indeed our data (Figures 5, 6) indicate that with increasing chain length the variations of the quantities mentioned above (fraction of adsorbed monomers, position of chain end, internal energy, chain linear dimensions) become more rapid in the transition region, and their fluctuations strongly increase. However, still longer chains would be required to convincingly demonstrate the expected finite size scaling. The distribution functions (Figure 8) are compatible with the fact that there is no significant free energy barrier separating the adsorbed and desorbed state, as predicted.<sup>32,64</sup> Note that at other first order phase transitions the barrier is due to the need to create interfaces associated with the nucleation of a droplet of the stable phase on the background of the metastable one. This is not the case here: the “interface” between the still adsorbed part of the macromolecule and the part that is already desorbed is a single monomer (or a few monomers, in the case of the bottle brushes). Thus, the hysteresis that we have found here (Figures

3, 4, and 9–11) is not related to the nucleation barrier in metastable states, unlike most other first order phase transitions. In the present type of systems, hysteresis can be observed since for (partially) adsorbed polymers conformational relaxation times can become very large, and hysteresis also can occur when the time constant associated with changing external control parameters of the system does not exceed these huge intrinsic conformational relaxation times of polymer systems. Thus, the hysteresis loops become steadily narrower when the time constant associated with the change of  $f$  increases. This narrowing would be by no means so pronounced when ordinary phase changes were considered. While we find that the location of the force-induced desorption transition depends on the presence or absence of side chains (and their length  $N$ , see Figure 12), we find that the part of the extension versus force curve where an essentially fully desorbed bottle brush is stretched further is almost independent of the presence of side chains. This means that the effective elastic modulus resisting the further extension is controlled by the backbone only. This part of the extension versus force curve can be well fitted by a formula proposed by Odijk.<sup>65</sup> The latter observation was also made in a recent experiment.<sup>20</sup> However, the experiment did not study how the behavior depends on side chain length yet. Thus, we hope that the present work will be useful for the interpretation of corresponding experiments.

## AUTHOR INFORMATION

### Corresponding Author

\*E-mail: (H.-P.H.) hsu@uni-mainz.de.

### Notes

The authors declare no competing financial interest.

## ACKNOWLEDGMENTS

One of us (H.-P. H) acknowledges support from the Deutsche Forschungsgemeinschaft (DFG), grant No SFB 625/A3. Useful discussions with W. Lechner are also acknowledged. We are also grateful to the NIC Jülich for a generous grant of computing time at the Jülich Supercomputing Centre (JSC).

## REFERENCES

- (1) Smith, S. B.; Finzi, L.; Bustamante, C. *Science* **1992**, *258*, 1112.
- (2) Perkins, T. T.; Smith, D. E.; Chu, S. *Science* **1994**, *264*, 819.
- (3) Florin, E. L.; Moy, V. T.; Gaub, H. E. *Science* **1994**, *264*, 415.
- (4) Strick, T. R.; Allemand, J.-F.; Bensimon, D.; Bensimon, A.; Croquette, V. *Science* **1996**, *271*, 1835.
- (5) Smith, S. B.; Cui, Y.; Bustamante, C. *Science* **1997**, *271*, 795.
- (6) Tskhovrebova, L.; Trinick, J.; Sleep, J. A.; Simmons, R. M. *Nature* **1997**, *387*, 308.
- (7) Rief, M.; Gautel, M.; Oesterhelt, F.; Fernandez, J. M.; Gaub, H. E. *Science* **1997**, *276*, 1109.
- (8) Essevaz-Roulet, B.; Bockelmann, U.; Hezlot, F. *Proc. Natl. Acad. Sci. U.S.A.* **1997**, *94*, 11935.
- (9) Kellermayer, M. S. Z.; Smith, S. B.; Granzier, H. L.; Bustamante, C. *Science* **1997**, *276*, 1112.
- (10) Oberhauser, A. F.; Marszalek, P. E.; Erickson, H. P.; Fernandez, J. M. *Nature* **1998**, *393*, 181.
- (11) Kreuzer, H. J.; Grunze, M. *Europhys. Lett.* **2001**, *55*, 640.
- (12) Bockelmann, U.; Thomen, Ph.; Essevaz-Roulet, B.; Viasnoff, V.; Heslot, F. *Biophys. J.* **2002**, *82*, 1537.
- (13) Liphardt, J.; Dumont, S.; Smith, S. B.; Tinoco, I.; Bustamante, C. *Science* **2002**, *296*, 1832.
- (14) Holland, N. B.; Hugel, T.; Neuert, G.; Cattani-Scholz, A.; Renner, C.; Oesterhelt, D.; Moroder, L.; Seitz, M.; Gaub, H. E. *Macromolecules* **2003**, *36*, 2015.
- (15) Douarche, F.; Ciliberto, S.; Petrosyan, A.; Rabbiosi, I. *Europhys. Lett.* **2005**, *70*, 593.
- (16) Hugel, T.; Rief, M.; Seitz, M.; Gaub, H. E.; Netz, R. R. *Phys. Rev. Lett.* **2005**, *94*, 048301.
- (17) Serr, A.; Netz, R. R. *Europhys. Lett.* **2006**, *73*, 292.
- (18) Kühner, F.; Erdmann, M.; Gaub, H. E. *Phys. Rev. Lett.* **2006**, *97*, 218301.
- (19) Neuert, G.; Hugel, T.; Netz, R. R.; Gaub, H. E. *Macromolecules* **2006**, *39*, 789.
- (20) Gunari, N.; Schmidt, M.; Janshoff, A. *Macromolecules* **2006**, *39*, 2219.
- (21) Harris, N. C.; Song, Y.; Kiang, C.-H. *Phys. Rev. Lett.* **2007**, *99*, 068101.
- (22) Strick, T. R.; Dessinges, M.-N.; Charvin, G.; Dekker, N. H.; Allemand, J.-F.; Bensimon, D.; Croquette, V. *Rep. Prog. Phys.* **2003**, *66*, 1.
- (23) Jarzynski, C. *Phys. Rev. Lett.* **1997**, *78*, 2690.
- (24) Jarzynski, C. *Phys. Rev. E* **1997**, *56*, 5018.
- (25) Crooks, G. E. *J. Stat. Phys.* **1998**, *90*, 1481.
- (26) Crooks, G. E. *Phys. Rev. E* **1999**, *60*, 2721.
- (27) Hummer, G.; Szabo, A. *Proc. Natl. Acad. Sci. U.S.A.* **2001**, *98*, 3658.
- (28) Wu, D.; Kofke, D. A. *J. Chem. Phys.* **2004**, *121*, 8742.
- (29) Wu, D.; Kofke, D. A. *J. Chem. Phys.* **2005**, *122*, 204104.
- (30) Jarzynski, C. *Phys. Rev. E* **2006**, *73*, 046105.
- (31) Jarzynski, C. *Eur. Phys. J. B* **2008**, *64*, 331.
- (32) Klushin, L. I.; Skvortsov, A. M. *J. Phys. A: Math. Theor.* **2011**, *44*, 473001.
- (33) Zhang, M.; Müller, A. H. E. *J. Polym. Sci., Part A, Polym. Chem.* **2005**, *43*, 3461.
- (34) Sheiko, S. S.; Sumerlin, B. S.; Matyjaszewski, K. *Prog. Polym. Sci.* **2008**, *33*, 759.
- (35) Rathgeber, S.; Pakula, T.; Wilk, A.; Matyjaszewski, K.; Beers, K. L. *J. Chem. Phys.* **2005**, *122*, 124904.
- (36) Zhang, B.; Gröhn, F.; Pedersen, J. S.; Fischer, K.; Schmidt, M. *Macromolecules* **2006**, *39*, 8440.
- (37) Hsu, H.-P.; Rathgeber, S.; Paul, W.; Binder, K. *Macromolecules* **2010**, *43*, 1592.
- (38) Hsu, H.-P.; Paul, W.; Binder, K. *Macromolecules* **2010**, *43*, 3094.
- (39) Hsu, H.-P.; Paul, W.; Binder, K. *Maromol. Theory Simul.* **2011**, *20*, 510.
- (40) Hsu, H.-P.; Paul, W.; Bnder, K. *J. Chem. Phys.* **2010**, *133*, 134902.
- (41) Hsu, H.-P.; Paul, W.; Binder, K. *J. Phys. Chem. B* **2011**, *115*, 14116.
- (42) Israilewitz, B.; Izrailev, S.; Schulten, K. *Biophys. J.* **1997**, *73*, 2972.
- (43) Gullingsrud, J. R.; Braun, R.; Schulten, K. *J. Comput. Phys.* **1999**, *151*, 190.
- (44) Israilewitz, B.; Gao, M.; Schulten, K. *Curr. Opin. Struct. Biol.* **2001**, *11*, 224.
- (45) Park, S.; Khalili-Araghi, F.; Tajkhorshid, E.; Schulten, K. *J. Chem. Phys.* **2003**, *119*, 3559.
- (46) Amaro, R.; Luthey-Schulten, Z. *Chem. Phys.* **2004**, *307*, 147.
- (47) Bhattacharya, S.; Rostiashvili, V. G.; Milchev, A.; Vilgis, T. A. *Macromolecules* **2009**, *42*, 2236.
- (48) Bhattacharya, S.; Milchev, A.; Rostiashvili, V. G.; Vilgis, T. A. *Phys. Rev. E* **2009**, *79*, 030802 (R).
- (49) Bhattacharya, S.; Rostiashvili, V. G.; Milchev, A.; Vilgis, T. A. *Eur. Phys. J. E* **2009**, *29*, 285.
- (50) Carmesin, I.; Kremer, K. *Macromolecules* **1998**, *21*, 2819.
- (51) Deutsch, H. P.; Binder, K. *J. Chem. Phys.* **1991**, *94*, 2294.
- (52) Paul, W.; Binder, K.; Heermann, D. W.; Kremer, K. *J. Phys. II* **1991**, *1*, 37.
- (53) Staple, D. B.; Geisler, M.; Hugel, T.; Kreplak, L.; Kreuzer, H. J. *New J. Phys.* **2011**, *13*, 013025.
- (54) Paturej, J.; Milchev, A.; Rostiashvili, V. G.; Vilgis, T. A. *Macromolecules* **2012**, *45*, 4371.
- (55) Binder, K. *Rep. Prog. Phys.* **1997**, *60*, 487.

- (56) Wittmer, J. P.; Beckrich, P.; Meyer, H.; Cavallo, A.; Johnner, A.; Baschnagel, J. *Phys. Rev. E* **2007**, *76*, 011803.
- (57) Binder, K., Ed. *Monte Carlo and Molecular Dynamics Simulations in Polymer Sciences*; Oxford Univ. Press: New York, 1995.
- (58) Binder, K.; Paul, W. *Polym. Sci., Part B: Polym. Phys.* **1997**, *35*, 1.
- (59) Doi, M., Edwards, S. F., *The Theory of Polymer Dynamics*; Clarendon Press: Oxford, U.K., 1986.
- (60) Hsu, H.-P.; Paul, W.; Binder, K. *EPL* **2010**, *92*, 28003.
- (61) Kratky, O.; Porod, G. *J. Colloid. Sci.* **1949**, *4*, 35.
- (62) Hsu, H.-P.; Binder, K.; Paul, W. *Polymer Sci. C* **2013**, *55*, 39.
- (63) Paul, W.; Binder, K.; Heermann, D. W.; Kremer, K. *J. Chem. Phys.* **1991**, *95*, 7726.
- (64) Skvortsov, A. M.; Klushin, L. I.; Polotsky, A. A.; Binder, K. *Phys. Rev. E* **2012**, *85*, 031803.
- (65) Odijk, T. *Macromolecules* **1995**, *28*, 7016.